

## Rotational Analysis of the BaI $C^2\Pi-X^2\Sigma^+$ Band System for the $\Delta v = 0$ Progression ( $v \leq 12$ )

CHRISTINE A. LEACH,<sup>1</sup> ATHANASSIOS A. TSEKOURAS, AND RICHARD N. ZARE

*Department of Chemistry, Stanford University, Stanford, California 94305*

High-resolution spectra of the  $P_{12}$ -,  $R_1$ -,  $P_2$ -, and  $R_{21}$ -branch members of the BaI  $C^2\Pi-X^2\Sigma^+$  ( $v, v$ ) bands with  $v = 0, 1, 4, 8$ , and 12 have been recorded using selectively detected laser-induced fluorescence (SDLIF). In addition, transitions involving high  $J''$  levels have been observed by undispersed fluorescence in the  $P_{12}$  and  $P_2$  branches of the (0, 0), (1, 1), (2, 2), and (3, 3) bands, and near the bandheads in the  $P_1$ ,  $Q_{12}$ ,  $P_{21}$ , and  $Q_2$  branches of the (0, 0) band. These data are combined with earlier optical measurements of the same electronic band system by Johnson *et al.*, Leach *et al.*, and Zhao *et al.*, and with microwave measurements of low  $J''$  levels for  $v = 0-5$  of the  $X^2\Sigma^+$  state by Törring and Döbl. Spectroscopic constants are obtained for the  $C^2\Pi$  and  $X^2\Sigma^+$  states using a weighted nonlinear least-squares fit to the optical and microwave transition wavenumbers, and bandhead positions for  $v \leq 12$ . The present set of 31 constants reproduces the positions of 5032 optical transitions with a standard deviation of  $2.4 \times 10^{-3} \text{ cm}^{-1}$ . No frequency perturbations are observed in our data. © 1992 Academic Press, Inc.

### 1. INTRODUCTION

The rotational analysis of electronic states in diatomic molecules has reached a stage of considerable maturity. Many electronic states have been studied at high resolution and analyzed to yield spectroscopic constants ( $I$ ). Yet, molecular band systems remain for which a rotational analysis is lacking because of a variety of different reasons. First, the molecule may be highly reactive requiring special techniques to generate it and then only in small numbers. Second, extensive perturbations and/or severe overlap of lines in the spectrum, may render interpretation almost impossible. The study of the BaI  $C^2\Pi-X^2\Sigma^+$  electronic transition is an example where the molecule is difficult to generate, being a radical, and where the spectrum is extremely congested.

The BaI  $C^2\Pi-X^2\Sigma^+$  spectrum was first identified by Walters and Barratt (2). More detailed vibrational analyses were carried out by Patel and Shah (3) and by Rao *et al.* (4). These studies showed that the spin-orbit interaction in the  $C^2\Pi$  state is large ( $756 \text{ cm}^{-1}$ ), such that the  $C^2\Pi-X^2\Sigma^+$  transition is observed as two well-separated subbands. In addition, the vibrational bands are separated by less than  $6 \text{ cm}^{-1}$ . These experiments were unable to resolve individual rotational transitions, which are very closely spaced, mainly because the large masses of the Ba and I atoms result in small rotational constants.

The electron excited in the  $C^2\Pi-X^2\Sigma^+$  transition moves between two nonbonding orbitals; thus, the bond length changes little on excitation resulting in both strong  $\Delta v = 0$  sequences with closely spaced vibrational bands (as already mentioned) and similar magnitudes for the rotational constants of the two states [ $B' \approx B'' \approx 0.027 \text{ cm}^{-1}$  (5)]. In addition, the spin-rotation splitting of the ground state and the  $\Lambda$ -doubling

<sup>1</sup> Present address: Department of Chemistry, University of Southampton, Southampton, Hampshire SO9 5NH, United Kingdom.

of the excited state result in six rotational branches per subband. The existence of these six different branches per subband, the small separation between vibrational bands, the very small rotational constants, and hyperfine effects lead to many overlapping transitions. Special techniques must be used to obtain spectra in which single branches can be identified and measured. Even applying laser-induced fluorescence (LIF) to the  $C^2\Pi-X^2\Sigma^+$  transition with a high-resolution continuous-wave laser does not allow the measurement of single rotational lines because of extensive overlap of different branches. The only exceptions to this are at the lowest frequency end of each subband, where it is possible for the laser to excite only one branch, and very close to a bandhead, where the transitions leading to the bandhead dominate the spectrum. Consequently, modifications of the standard LIF technique must be employed to obtain rotational resolution. Two such techniques have been used in the studies of BaI, motivated by the desire to understand the kinematically constrained reaction  $Ba + HI \rightarrow BaI + H$  (6, 7).

One technique is population-labeling optical-optical double resonance (PLOODR) (8, 9), which has been used to assign a number of rovibronic transitions in the (0, 0) (5, 9) and (8, 8) (10) bands. The other technique is selectively detected laser-induced fluorescence (SDLIF) (11), which has yielded most of the data previously recorded for BaI (5, 10, 12). This latter technique was used extensively to obtain the new data described in this paper.

In addition, some information is available on the structure of the BaI ground state. Törring and Döbl (13) measured 24 microwave transitions between different rotational levels in the  $X^2\Sigma^+$  state. Their data involved vibrational levels up to  $v = 5$  and rotational levels in the region of  $J = 60.5$ .

In this paper we combine the results from these earlier studies (5, 10, 12, 13) with new measurements on the (0, 0), (1, 1), (2, 2), (3, 3), (4, 4), (8, 8), and (12, 12) bands. We find that one set of spectroscopic constants is able to reproduce satisfactorily all the observed transitions.

## 2. EXPERIMENTAL DETAILS

### (a) *Selectively Detected Laser-Induced Fluorescence (SDLIF)*

The majority of the new transitions have been measured by SDLIF. The experimental setup has been described previously (12). In brief, HI gas at a pressure of about  $8 \times 10^{-4}$  Torr reacts with a beam of Ba from an oven source maintained at 1300 K. A ring dye laser (Coherent 699-29) with a power of approximately 20 mW crosses the Ba beam at  $90^\circ$  and excites product BaI molecules in the  $C^2\Pi-X^2\Sigma^+$  band system as the frequency is scanned. The transitions are detected by collecting the fluorescence through a monochromator perpendicular to the excitation laser beam. The Doppler width with this setup is 250 MHz. The monochromator entrance and exit slits are typically set to 200  $\mu\text{m}$ , which corresponds to a transmission full-width at half-maximum (FWHM) of about  $6 \text{ cm}^{-1}$ . The monochromator transmission function is set at a fixed wavenumber to collect fluorescence from transitions that have a common upper level with those being excited and is made narrow enough to isolate one branch from neighboring branches in other vibrational bands.

### (b) *Undispersed Fluorescence Measurements*

As already mentioned, at the lowest frequency end of each  $\Delta v = 0$  subband that corresponds to low vibrational levels, the laser excites only one branch,  $P_{12}$  or  $P_2$ .

Thus, these branches can be measured by LIF in which the undispersed fluorescence is detected. A full description of our crossed beam apparatus has been presented (14) and details of its use in spectroscopic measurements have been described (12).

In these experiments a supersonic HI beam is formed by expansion of a mixture of 6% HI in a carrier gas ( $N_2$  and/or Ar/He). This HI beam crosses the Ba beam at  $90^\circ$ . The ring dye laser beam, with a power of 5 mW (to avoid saturation) crosses the interaction region perpendicular to the plane containing the Ba and HI beams and excites product BaI molecules in the  $C^2\Pi-X^2\Sigma^+$  transition. The undispersed fluorescence is collected by a photomultiplier situated in the plane containing the Ba and HI beams (i.e., perpendicular to the excitation laser beam).

### (c) Absolute Frequency Calibration

In all our spectroscopic measurements,  $I_2$  absorption spectra recorded simultaneously with the BaI spectra are used for absolute calibration of the measured wavenumbers (15). This calibration gives an accuracy of  $0.003\text{ cm}^{-1}$  on uncontaminated lines.

## 3. RESULTS

A Fortrat diagram for the BaI  $C^2\Pi_{3/2}-X^2\Sigma^+$  (12, 12) subband is shown in Fig. 1a. All other  $C^2\Pi_{3/2}-X^2\Sigma^+$  ( $v, v$ ) subbands are similar in structure but are shifted, as can be seen Fig. 1b where the (10, 10) to (14, 14) subbands are added to the (12, 12) subband. The band origins are separated by only  $5.6\text{ cm}^{-1}$ . This also illustrates why extensive overlap of different branches occurs in the BaI  $C^2\Pi-X^2\Sigma^+$  spectrum; rotational levels in  $v = 12$  up to at least  $J'' = 300.5$  are populated under beam-gas conditions. The  $C^2\Pi_{1/2}-X^2\Sigma^+$  subband has exactly the same structure except that it is  $756\text{ cm}^{-1}$  lower in wavenumber. The corresponding branch labels for the  $C^2\Pi_{1/2}-X^2\Sigma^+$  subband in order of increasing wavenumber are  $P_{12}, P_1, Q_{12}, Q_1, R_{12},$  and  $R_1$ .

Figure 1a also shows how SDLIF is applied to measure  $R_{21}$ -branch members of the (12, 12) band. The  $R_{21}(J)$  branch shares common upper levels with the ( $P_{21}(J+2), Q_2(J+1)$ ) branches, where the parentheses are used to denote a pair of closely spaced branches on the Fortrat diagram. Thus to measure the (12, 12)  $R_{21}$  branch the laser is scanned over the wavenumbers shown while the monochromator "detection window" is set to collect fluorescence from the (12, 12) ( $P_{21}, Q_2$ ) branches. A spectrum recorded using this arrangement is shown in Fig. 2a. In a similar manner the (12, 12)  $P_2$  branch shown in Fig. 2b was recorded by scanning the laser along the (12, 12)  $P_2$  branch and collecting fluorescence from the (12, 12) ( $Q_{21}, R_2$ ) branches.

SDLIF allows the measurement of only 4 of the 12 possible branches in each vibrational band. These are the outer  $P_2$  and  $R_{21}$  branches on the Fortrat diagram [see Fig. 1a], and the equivalent  $P_{12}$  and  $R_1$  branches of the other spin-orbit subband. There is a limit on the lowest  $J''$  that can be measured by selective detection. Once the transmission function includes the excitation wavenumber, the fluorescence will no longer be selectively detected. The lowest  $J''$  we have recorded by this method is 41.5. The pairs of branches that occur almost on top of each other, ( $P_1, Q_{12}$ ), ( $Q_1, R_{12}$ ), ( $P_{21}, Q_2$ ), and ( $Q_{21}, R_2$ ) cannot be recorded by SDLIF with our experimental setup.  $Q_1$ - and  $Q_{12}$ -branch members were recorded by SDLIF in the (0, 0) (5) and (8, 8) (10) bands. These  $Q$  branches could be recorded because  $Q$ -branch transitions to the  $C^2\Pi_{1/2}$  state are about five times stronger than the  $P$ - or  $R$ -branch transitions. This intensity difference is because of different hyperfine splittings and transition probabilities between the  $Q$  and  $P/R$  branches. Those earlier experiments (5, 10) differ

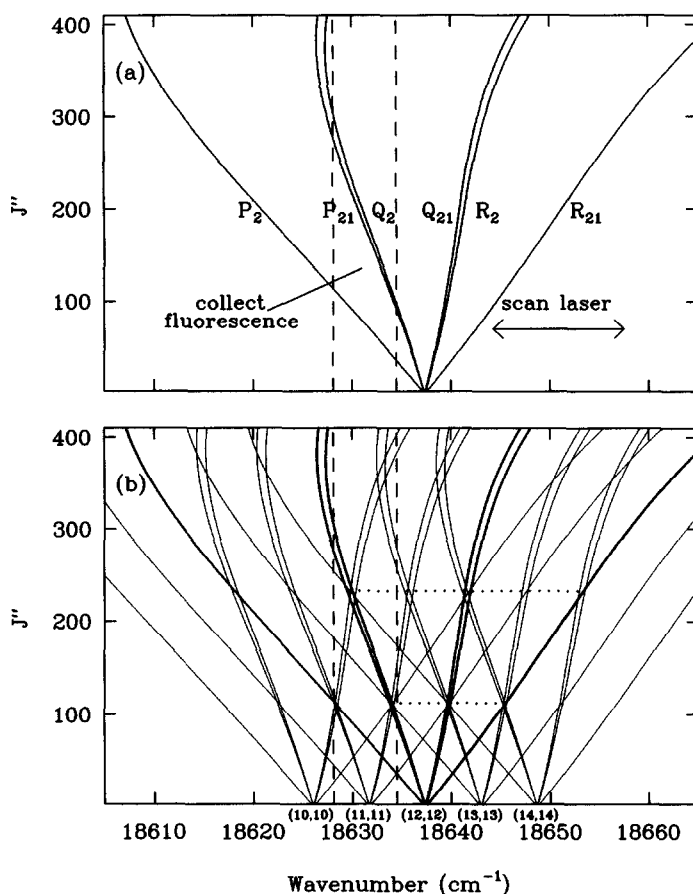


FIG. 1. (a) Fortrat diagram of the BaI  $C^2\Pi_{3/2}-X^2\Sigma^+$  (12, 12) subband illustrating selective detection of the  $R_{21}$  branch. The dashed lines show the monochromator "detection window." (b) As (a) but with the (10, 10) to (14, 14) subbands added. Two positions of contamination of the (12, 12)  $R_{21}$  branch are shown by dotted lines.

from ours in the use of a beam of BaI from an oven. As a result, the Doppler width of the transitions was smaller (20–150 MHz) than in our beam-gas reaction. With our broader Doppler width from the beam-gas reaction we have been unable to see sequences in any  $Q$  branch.

At certain wavenumbers in the SDLIF spectra, it is impossible to avoid interferences from other branches, even in the  $P_{12}$ ,  $R_1$ ,  $P_2$ , and  $R_{21}$  branches. Several of these interferences are clearly visible in the spectra in Fig. 2; they appear as broad peaks causing rises in the baseline. The origins of the interferences in the  $R_{21}$  branch are illustrated in the Fortrat diagram in Fig. 1b. The lower wavenumber interference is caused by the (13, 13) ( $Q_{21}$ ,  $R_2$ ) branches at a  $J''$  of about 120.5. This interference is observed because these ( $Q_{21}$ ,  $R_2$ )-branch members fluoresce in the (13, 13)  $P_2$  branch at a wavenumber collected by the monochromator. The higher wavenumber interference is from the (14, 14) ( $Q_{21}$ ,  $R_2$ ) branches. The width of these interferences can be reduced by narrowing the monochromator slits at the cost of decreasing the signal but they cannot be completely eliminated. The interferences that appear in the  $P_2$

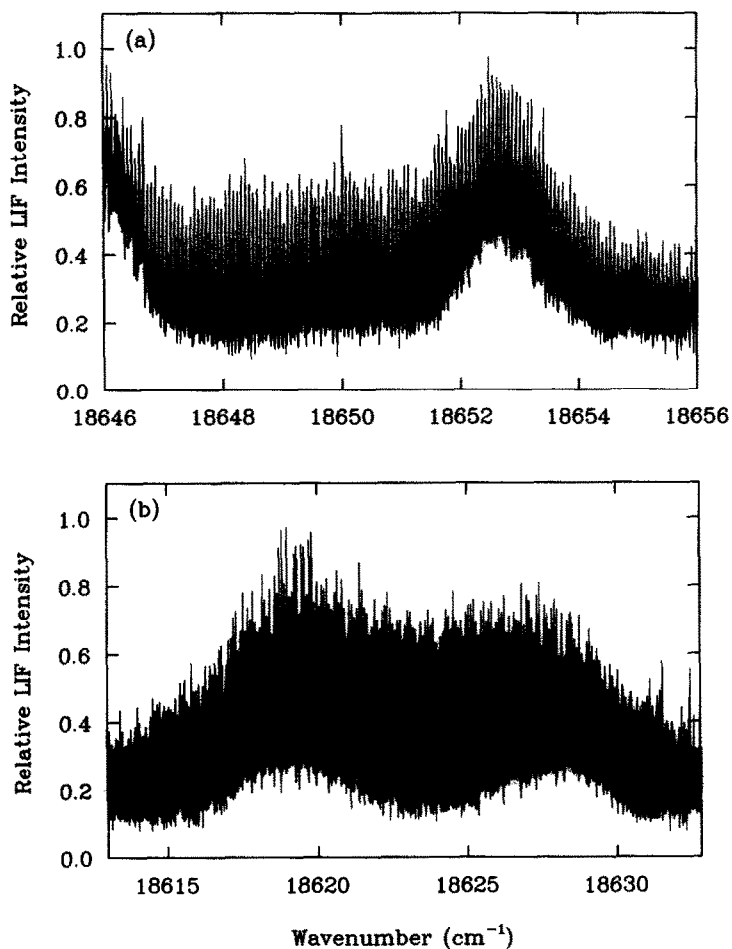


FIG. 2. (a) SDLIF spectrum of the  $R_{21}$  branch of the BaI  $C^2\Pi_{3/2}-X^2\Sigma^+$  (12, 12) band for  $J''$  values between 120.5 and 286.5. (b) SDLIF spectrum of the  $P_2$  branch of the BaI  $C^2\Pi_{3/2}-X^2\Sigma^+$  (12, 12) band for  $J''$  values between 298.5 and 57.5.

branch shown in Fig. 2b are from the (10, 10) (lower wavenumber) and (11, 11) ( $P_{21}$ ,  $Q_2$ ) branches.

The two spectra in Fig. 2 also illustrate an interesting difference between the effects of the interferences on the two branches. In Fig. 2a the interferences are from ( $Q_{21}$ ,  $R_2$ )-branch members which are so closely spaced that they overlap. In these branches a point of inflection occurs on the Fortrat diagram. Therefore, in this spectrum the interferences are observed as a smoothly rising baseline upon which the structure of the  $R_{21}$ -branch members is superimposed. On the other hand, in the  $P_2$  branch [Fig. 2b] the interferences are caused by ( $P_{21}$ ,  $Q_2$ )-branch members which are more widely spaced. In this case the baseline rise is not so smooth and structure from the interfering branches can be seen. Hence, measurement of the  $R_{21}$ -branch members in the regions of the interferences will be more accurate than those of the  $P_2$ -branch members.

In total we have measured more than 2000 transitions by SDLIF. A summary of the branches and rotational quantum numbers of the transitions measured is given in Table I.

TABLE I

Vibrational Band, Branch Assignment, and Range of  $J''$  Values for Transitions Measured

SDLIF Results			Undispersed Fluorescence Results		
Band	Branch	Range of $J''$	Band	Branch	Range of $J''$
(0, 0)	R <sub>1</sub>	142.5-377.5	(0, 0)	P <sub>1</sub>	404.5-431.5
(1, 1)	P <sub>2</sub>	44.5-467.5		Q <sub>12</sub>	353.5-531.5
(4, 4)	P <sub>2</sub>	114.5-423.5		P <sub>21</sub>	373.5-430.5
	R <sub>21</sub>	123.5-411.5		Q <sub>2</sub>	359.5-423.5
(8, 8)	R <sub>1</sub>	208.5-341.5	(1, 1)	P <sub>12</sub>	351.5-465.5
	R <sub>21</sub>	236.5-359.5		P <sub>2</sub>	341.5-468.5
	P <sub>2</sub>	41.5-354.5	(2, 2)	P <sub>12</sub>	337.5-447.5
(12, 12)	P <sub>12</sub>	104.5-232.5		P <sub>2</sub>	327.5-440.5
	R <sub>1</sub>	122.5-302.5	(3, 3)	P <sub>2</sub>	392.5-432.5
	P <sub>2</sub>	57.5-298.5		P <sub>12</sub>	356.5-420.5
	R <sub>21</sub>	67.5-286.5			

Between the (0, 0)  $P_2$  bandhead and the (1, 1)  $P_2$  bandhead the laser can only excite the (0, 0)  $P_2$  branch. In this region the (0, 0)  $P_2$  branch can therefore be measured by undispersed fluorescence whether the BaI is produced by crossed-beam or beam-gas reactions. The crossed-beam reaction of Ba with HI was found to produce narrow, very highly excited rotational distributions (7). Because the population distributions are so narrow, high  $J''$  members of the  $P_2$  (1, 1), (2, 2), and (3, 3) branches can be identified in an undispersed fluorescence spectrum and have been measured. Figure 3 shows the (2, 2)  $P_2$  branch between  $J''$  about 340.5 and 440.5. Just above 18,550  $\text{cm}^{-1}$  the (2, 2)  $P_2$  branch is no longer visible and the (3, 3)  $P_2$  branch starts to gain intensity. At the right edge the strong (0, 0)  $P_2$  bandhead appears and no more (3, 3)  $P_2$  branch members can be seen. The above conclusions apply equally well to the other spin-orbit subband where members of the  $P_{12}$  branch have been measured for

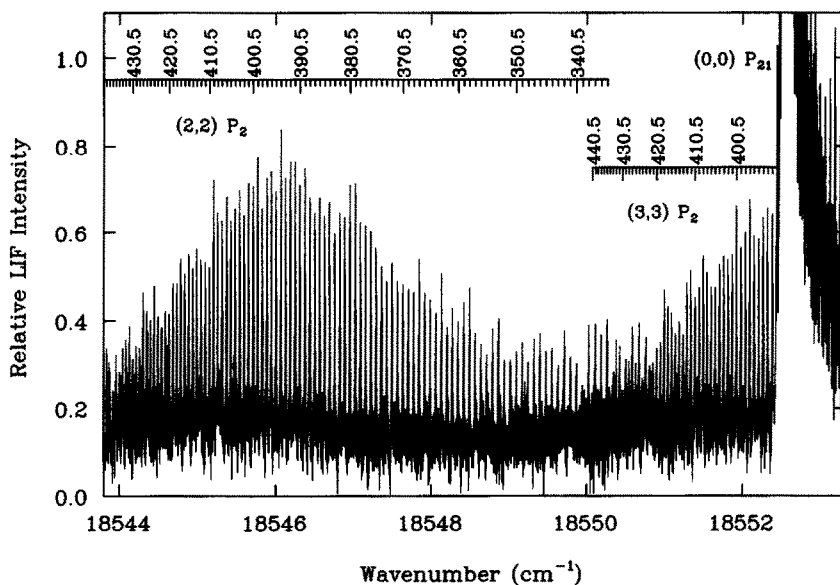


FIG. 3. Undispersed fluorescence spectrum of the BaI  $C^2\Pi_{3/2}-X^2\Sigma^+$  subband showing (2, 2)  $P_2$  branch members, a few (3, 3)  $P_2$  branch members, and the strong (0, 0)  $P_{21}$  bandhead.

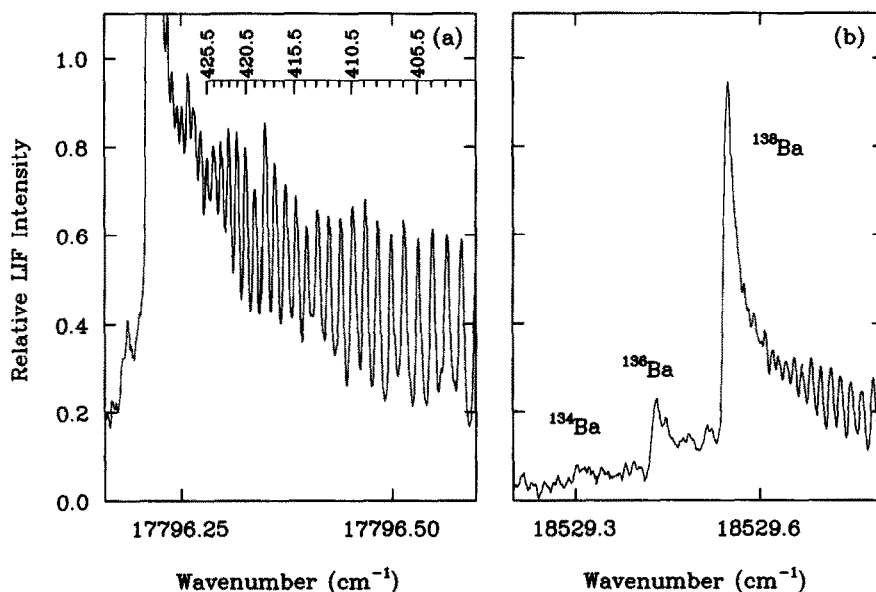


FIG. 4. (a) Undispersed fluorescence spectrum of the BaI  $C^2\Pi_{3/2}-X^2\Sigma^+(0,0) Q_{12}$  bandhead and  $(0,0) Q_{12}$  branch members just below the bandhead. (b) Undispersed fluorescence spectrum of the  $^4\text{BaI } C^2\Pi_{3/2}-X^2\Sigma^+(0,0) P_2$  bandheads for  $A = 134, 136,$  and  $138$ .

$(0,0), (1,1), (2,2),$  and  $(3,3)$ . Table I lists the branches measured with their assignments.

Close to the bandheads in the  $(0,0)$  band lines appear that can be identified as belonging to the same branch as the bandhead. An example of the  $Q_{12}(0,0)$  bandhead and  $Q_{12}$  transitions are shown in Fig. 4a. High  $J''$  transitions in the  $(0,0) P_1, Q_{12}, P_{21},$  and  $Q_2$  branches have been measured near their bandheads. The  $J''$  values of those measured are also given in Table I. Several long-range scans have been carried out under crossed-beam conditions with undispersed fluorescence collection. Bandhead positions for the  $P_{12}, P_1, Q_{12}, P_2, P_{21},$  and  $Q_2$  branches of the  $\Delta v = 0$  progression have been measured up to a maximum  $v$  of 35 and are presented in Table II.

#### 4. ANALYSIS

The  $C^2\Pi$  and  $X^2\Sigma^+$  Hamiltonians have been described in detail elsewhere (16, 17). The effective Hamiltonian for a vibrating-rotating diatomic molecule may be written

$$H = H_0 + H_{\text{rot}} + H_{\text{fs}} + H_{\text{hfs}}, \quad (1)$$

where  $H_0$  contains terms that only depend on the electronic,  $n$ , and vibrational,  $v$ , state of the molecule;  $H_{\text{rot}}$  is the rotational Hamiltonian;  $H_{\text{fs}}$  is the fine-structure Hamiltonian; and  $H_{\text{hfs}}$  contains terms involving nuclear spin which give rise to the hyperfine structure.  $H_{\text{hfs}}$  is ignored in the following analysis because hyperfine splittings are not resolved, although evidence for hyperfine effects can be seen in the lineshapes. The hyperfine effects of the  $X^2\Sigma^+$  and  $C^2\Pi$  states of BaI have been measured by Ernst *et al.* (18).

$H_{\text{rot}}$  has the form  $H_{\text{rot}} = B(r)(\mathbf{J} - \mathbf{L} - \mathbf{S})^2$  (16), where  $\mathbf{J}$  is the total angular momentum omitting nuclear spin,  $\mathbf{L}$  is the electronic orbital angular momentum, and

TABLE II

Wavenumbers of Experimental Bandhead Positions and Differences from Calculated Positions

Branch (v,v)	Expt (cm <sup>-1</sup> )	Expt-Calc. (cm <sup>-1</sup> )	Branch (v,v)	Expt (cm <sup>-1</sup> )	Expt-Calc. (cm <sup>-1</sup> )
P <sub>12</sub>	0	17775.076	P <sub>21</sub>	0	18552.498
	1	17781.361		1	18558.765
	2	17787.637		2	18565.014
	3	17793.881		3	18571.249
P <sub>1</sub>	4	17800.125	4	18577.462	
	0	17795.127	5	18583.655	
	1	17801.232	6	18589.832	
	2	17807.322	7	18595.988	
	3	17813.388	8	18602.126	
	4	17819.441	9	18608.245	
	5	17825.473	10	18614.341	
	6	17831.482	11	18620.430	
	7	17837.477	12	18626.492	
	8	17843.455	13	18632.535	
	9	17849.416	14	18638.562	
	10	17855.348	15	18644.568	
	11	17861.263	16	18650.555	
	12	17867.163	17	18656.524	
	13	17873.044	18	18662.473	
	14	17878.908	19	18668.403	
	15	17884.749	20	18674.311	
	16	17890.572	21	18680.203	
17	17896.377	22	18686.071		
18	17902.161	23	18691.921		
Q <sub>12</sub>	0	17796.210	24	18697.751	
	1	17802.301	25	18703.559	
	2	17808.376	26	18709.338	
	3	17814.431	27	18715.113	
	4	17820.465	28	18720.859	
	5	17826.481	29	18726.583	
	6	17832.480	30	18732.280	
	7	17838.458	31	18737.953	
	8	17844.419	32	18743.607	
	9	17850.361	33	18749.235	
	10	17856.282	34	18754.834	
	11	17862.186	35	18760.407	
	12	17868.072	Q <sub>2</sub>	0	18553.569
	13	17873.937		1	18559.823
	14	17879.786		2	18566.054
	15	17885.613		3	18572.267
	16	17891.421		4	18578.466
	17	17897.212		5	18584.643
18	17902.984	6		18590.804	
P <sub>2</sub>	0	18529.547		7	18596.941
	1	18536.062		8	18603.063
	2	18542.555		9	18609.171
	3	18549.029		10	18615.252
	4	18555.485		11	18621.318
	5	18561.921		12	18627.365
	6	18568.334		13	18633.414
	7	18574.735		14	18639.410
	8	18581.115		15	18645.501
	9	18587.475	16	18651.363	
10	18593.819				

$S$  is the electronic spin angular momentum. The fine-structure Hamiltonian contains two terms that need to be considered in the doublet states of BaI. The  $C^2\Pi$  state has a spin-orbit interaction given by  $A(r)L \cdot S$  and the  $X^2\Sigma^+$  state has a spin-rotation interaction given by  $\gamma(r)N \cdot S$ , where  $N = J - S$ . Hund's coupling case (a) wavefunctions are used in our analysis. In this basis set the wavefunctions are eigenfunctions of  $J^2$ ,  $S^2$ ,  $J_z$ ,  $S_z$ , and  $L_z$  with eigenvalues  $J(J+1)$ ,  $S(S+1)$ ,  $\Omega$ ,  $\Sigma$ , and  $\Lambda$ . The matrix elements of these operators in the same  $|nvJSA\rangle$  block have been evaluated (16). These are written in terms of the following spectroscopic constants: the band origin,  $T_v$ , rotational constant,  $B_v$ , spin-orbit constant,  $A_v$ , and spin-rotation constant,  $\gamma_v$ . Off-diagonal elements between different  $|nvJSA\rangle$  blocks are required because of

the radial dependence of the operators in the Hamiltonian. These are included as additional correction terms in the  $|nvJ\Lambda\rangle$  blocks which are calculated by means of a van Vleck transformation (16, 17, 19). Thus centrifugal distortion corrections caused by coupling between different vibrational blocks give rise to terms involving the spectroscopic constants  $D_v$ ,  $A_{Dv}$ , and  $\gamma_{Dv}$ , where  $D_v$  is the centrifugal distortion correction to  $B_v$ ,  $A_{Dv}$  to  $A_v$ , and  $\gamma_{Dv}$  to  $\gamma_v$ . Corrections arising from coupling between different electronic blocks cause  $\Lambda$ -doubling effects characterized by the  $\Lambda$ -doubling parameters  $p_v$ ,  $q_v$ , and  $o_v$  and their centrifugal distortion corrections,  $p_{Dv}$ ,  $q_{Dv}$ , and  $o_{Dv}$ .  $o_v$  and  $o_{Dv}$  cannot be determined independently because they are completely correlated with other terms; they are set to zero in our analysis. The BaI  $C^2\Pi-X^2\Sigma^+$  spectra have been measured to such high rotational excitation ( $J''_{\max} = 531.5$ ) that higher-order corrections are also required to fit the data. The higher-order centrifugal distortion corrections included in our analysis are  $H_v$ , the correction to  $B_v$ , and  $A_{Hv}$ , the correction to  $A_v$ .

A summary of the parameters used to describe each  $(v, v)$  band follows. The  $C^2\Pi-X^2\Sigma^+$   $(v, v)$  vibrational band origin,  $\nu_{vv}$ , is included for the  $\Delta v = 0$  transitions; this is equivalent to  $T'_v - T''_v$ . For the  $C^2\Pi$  state the spectroscopic constants included are the rotational constants,  $B'_v$ ,  $D'_v$ ,  $H'_v$ , the spin-orbit constants,  $A'_v$ ,  $A'_{Dv}$ ,  $A'_{Hv}$ , and the  $\Lambda$ -doubling constants,  $q'_v$ ,  $p'_v$ ,  $q'_{Dv}$ , and  $p'_{Dv}$ . For the  $X^2\Sigma^+$  state the rotational constants,  $B''_v$ ,  $D''_v$ , and  $H''_v$ , and the spin-rotation constants  $\gamma''_v$  and  $\gamma''_{Dv}$  are used.

The analysis using the Hamiltonians described above was extended to all vibrational levels simultaneously by using Dunham-type expansions (17, 20) of the above parameters, i.e., each constant is written as an expansion in  $v$  of the type

$$x_{vi} = x_{0i} + x_{1i}(v + \frac{1}{2}) + x_{2i}(v + \frac{1}{2})^2, \quad (2)$$

where  $x_v$  is any of the above spectroscopic constants. Quadratic terms were only included for  $\nu_{vv}$ ,  $B'_v$ ,  $B''_v$ ,  $D'_v$ , and  $A'_v$ .  $D''_v$ ,  $A'_{Dv}$ ,  $p'_v$ ,  $q'_v$ , and  $\gamma'_v$  were fit to linear expressions and the other parameters, which are very small were fixed independent of  $v$ . In this way we define

$$\nu_{vv} = \Delta v + \Delta\omega_e(v + \frac{1}{2}) + \Delta\omega_e x_e(v + \frac{1}{2})^2 \quad (3a)$$

$$B_v = Y_{01} + Y_{11}(v + \frac{1}{2}) + Y_{21}(v + \frac{1}{2})^2 \quad (3b)$$

$$-D_v = Y_{02} + Y_{12}(v + \frac{1}{2}) + Y_{22}(v + \frac{1}{2})^2 \quad (3c)$$

$$H_v = Y_{03} \quad (3d)$$

$$A_v = A_{00} + A_{10}(v + \frac{1}{2}) + A_{20}(v + \frac{1}{2})^2 \quad (3e)$$

$$A_{Dv} = A_{01} + A_{11}(v + \frac{1}{2}) \quad (3f)$$

$$A_{Hv} = A_{02}. \quad (3g)$$

The other parameters are expanded in the same way. The results in Table III show which parameters were included in the final fit. With the above definition of  $\nu_{vv}$  the parameter  $\Delta v = T'_e - T''_e + Y'_{00} - Y''_{00}$ ,  $\Delta\omega_e = \omega'_e - \omega''_e$ , and  $\Delta\omega_e x_e = \omega'_e x'_e - \omega''_e x''_e$ .

A weighted nonlinear least-squares fit to the experimental wavenumbers was used to determine the spectroscopic coefficients. Weights were assigned to the data as follows. The weight of each measured wavenumber is the reciprocal of the experimental standard deviation,  $\sigma$ . For the microwave data of Törring and Döbl,  $\sigma$  was taken to be 3

TABLE III

Molecular Constants in  $\text{cm}^{-1}$  for the Bal  $C^2\Pi-X^2\Sigma^+$  Band System for the  $\Delta v = 0$  Progression ( $v \leq 12$ )  
Determined from a Weighted Nonlinear Least-Squares Fit of the Data

$\Delta v$	$1.81884943(3) \times 10^{+4}$	$q_{00}^I$	$-1.374(328) \times 10^{-6}$
$\Delta\omega_e$	$5.63482(13) \times 10^0$	$q_{10}^I$	$5.43(398) \times 10^{-8}$
$\Delta\omega_e x_e$	$-2.5283(116) \times 10^{-3}$	$q_{01}^I$	$7.76(183) \times 10^{-12}$
$A_{00}^I$	$7.560594(5) \times 10^{+2}$	$P_{00}^I$	$7.0247(39) \times 10^{-3}$
$A_{10}^I$	$1.09045(148) \times 10^{-1}$	$P_{10}^I$	$-4.235(40) \times 10^{-5}$
$A_{20}^I$	$1.676(11) \times 10^{-3}$	$P_{01}^I$	$-3.224(31) \times 10^{-9}$
$A_{01}^I$	$-4.0716(108) \times 10^{-6}$	$Y_{01}^{II}$	$2.6805878(8) \times 10^{-2}$
$A_{11}^I$	$3.8206(107) \times 10^{-7}$	$Y_{11}^{II}$	$-6.6342(3) \times 10^{-5}$
$A_{02}^I$	$7.253(51) \times 10^{-12}$	$Y_{21}^{II}$	$3.397(32) \times 10^{-8}$
$Y_{01}^I$	$2.672800(17) \times 10^{-2}$	$Y_{00}^{II}$	$-3.3288(10) \times 10^{-9}$
$Y_{11}^I$	$-6.3610(22) \times 10^{-5}$	$Y_{12}^{II}$	$-1.31(29) \times 10^{-12}$
$Y_{21}^I$	$2.50(5) \times 10^{-8}$	$Y_{03}^{II}$	$-1.272(80) \times 10^{-16}$
$Y_{02}^I$	$-3.0726(14) \times 10^{-9}$	$\gamma_{00}^{II}$	$2.53294(36) \times 10^{-3}$
$Y_{12}^I$	$-1.693(295) \times 10^{-12}$	$\gamma_{10}^{II}$	$-1.124(11) \times 10^{-5}$
$Y_{22}^I$	$1.06(22) \times 10^{-14}$	$\gamma_{01}^{II}$	$-3.82(11) \times 10^{-10}$
$Y_{03}^I$	$-1.032(80) \times 10^{-16}$		

Numbers in parentheses represent two standard deviations in units of the last figure quoted.

$\times 10^{-7} \text{ cm}^{-1}$  (13). For the optical data, values of  $\sigma$  between  $3 \times 10^{-3}$  and  $7 \times 10^{-3} \text{ cm}^{-1}$  were used depending on the quality of the spectrum. A lower weight was assigned to transitions in spectra where interferences were visible from other branches. When the same transition was measured more than once, the weighted average of the position was calculated and the weight adjusted appropriately. The bandhead positions were assigned  $\sigma$  values of  $5 \times 10^{-3} \text{ cm}^{-1}$ .

The first question to be answered by the analysis is the uniqueness of the assignment. The earlier (0, 0) and (8, 8) work provided a definitive assignment for these two bands. In both cases these assignments were based on initial PLOODR experiments (8, 10). Additional assignments were made by counting branch members and extrapolating, if necessary. In the (0, 0) band we were able to assign  $P_{12}$ -branch members to  $J''$  values between 339.5 and 486.5, even though we had not observed any of the branch members between  $J''$  values of 115.5 and 339.5 (12). The previous assignments of the (0, 0) and (8, 8) bands combined with the microwave data of Törring and Döbl (13), which give precise information on the vibrational dependence of the parameters in the  $X^2\Sigma^+$  state, provided a starting point in the analysis.

First, the best nonlinear least-squares fit to the (0, 0), (8, 8), and microwave data was obtained; only linear vibrational dependences for the upper state parameters were required. The optimized set of spectroscopic constants was then used to simulate the next branch to be added to the fit. This assignment and those with the  $J''$ 's of the new branch reassigned by  $\pm 1$  were tested. In each case the spectroscopic constants were reoptimized, additional constants added, if necessary, and both the overall standard deviation of the fit and the residuals examined. For all the branches we had measured it was found that only one assignment was acceptable. Wrong assignments gave significant trends in the residuals and higher overall standard deviations. The branches were added to the data set in order of increasing  $v$ , and within each ( $v, v$ ) band the branch with the most data was added first. Thus, extrapolation to the (12, 12) band

was performed last. Even for this band only one assignment was satisfactory. (The bandheads did not require assignment of  $J''$ .)

After the members of all branches had been assigned, a weighted nonlinear least-squares fit was carried out including all 5032 optical and 24 microwave transition wavenumbers and the 68 ( $v, v$ ) bandhead positions for  $v \leq 12$ . The complete data set has been sent to the *Journal* for archive purposes. The results of the final fit are given in Table III with two sigma errors on each constant. The number of significant figures quoted are required to reproduce calculated transition wavenumbers, even though the constants are not determined to that accuracy (21). Addition of extra constants was examined to see if they made a significant difference to the fit; additional parameters do improve the fit, but it is already good enough to reproduce the experimental results within the expected accuracy. The parameters in Table III therefore represent the minimum set required to fit the data. The overall standard deviation of the final fit is  $2.37 \times 10^{-3} \text{ cm}^{-1}$ .

## 5. DISCUSSION

From our analysis we can determine the difference in the vibrational constants between the BaI  $C^2\Pi$  and  $X^2\Sigma^+$  states. The value for  $\Delta\omega_e$  of  $5.63 \text{ cm}^{-1}$  is in good agreement with earlier vibrational studies by Rao *et al.* (4). They were not able to determine  $\Delta\omega_e x_e$  to the order of  $\pm 0.003 \text{ cm}^{-1}$ , which is determined in our fit to be  $-0.0026 \text{ cm}^{-1}$ .

In our rotational analysis of the BaI  $C^2\Pi$ - $X^2\Sigma^+$   $\Delta v = 0$  bands we assume that there are no significant frequency perturbations in our data and that the spectroscopic constants vary smoothly with  $v$ . The successful results of the fitting procedure confirm these assumptions. Both the  $C^2\Pi$  and  $X^2\Sigma^+$  states of BaI have very similar potential energy curves, as is confirmed by the small values of  $\Delta\omega_e$  and  $\Delta\omega_e x_e$  and the similarity of the rotational constants. Up to  $v = 12$  most of the spectroscopic constants only show a small dependence on the vibrational quantum number. This is perhaps not surprising as the energy gap between successive vibrational levels is only approximately  $152 \text{ cm}^{-1}$  in the  $X^2\Sigma^+$  state and  $158 \text{ cm}^{-1}$  in the  $C^2\Pi$  state. The  $A_{Dv}$  constant shows a large dependence on  $v$ ;  $A_{11}$  is only 10 times smaller than  $A_{01}$  [see Eq. (3f)]. This behavior is a direct result of the (0, 0) and (8, 8) data, where fits of the individual vibrational bands give  $A_{D0} = -3.52 \times 10^{-6} \text{ cm}^{-1}$  and  $A_{D8} = -7.8 \times 10^{-7} \text{ cm}^{-1}$ , requiring a strong  $v$  dependence for  $A_{Dv}$ .

Two other spectroscopic constants are worthy of further comment.  $Y'_{22}$  was included in the fit but not  $Y''_{22}$  because the two parameters are highly correlated when both are included. The value of  $Y'_{22}$  should be regarded as  $Y'_{22} - Y''_{22}$  because their difference is determined better than either separately. The differences between the same upper and lower state rotational constant are all better determined than the absolute values of the rotational constants, which is why more significant figures are included in the results than justified by their uncertainties (21). The value of  $q'_0$  obtained from the fit is determined to be  $-1.3 \times 10^{-6} \text{ cm}^{-1}$ , which is a factor of seven smaller than the value determined previously in fitting the (0, 0) band (12). This is a consequence of including more data in the present analysis. Previously no high  $J''$  data were included in the (0, 0)  $Q_{12}$ ,  $P_1$ ,  $R_1$ ,  $Q_2$ , and  $P_{21}$  branches; thus  $q'_0$  is shown to be very sensitive to the exact data included. The new value is closer to the order of magnitude expected from the value of  $p'_0$  and an estimate from the unique perturber approximation (10, 12, 21).

The data analyzed are only a sample of all the possible transitions in the 12 branches of each  $\Delta v = 0$  band between  $v = 0$  and 12. They are also strongly biased in favor of the branches that can be measured by SDLIF ( $P_{12}$ ,  $R_1$ ,  $P_2$ , and  $R_{21}$ ). The parameters in Table III should give good predictions for these four branches at intermediate  $v$  values in  $\Delta v = 0$  bands. Accurate predictions of the other eight branches are not guaranteed.

In addition to the experimental bandhead positions of the  $P_{12}$ ,  $P_1$ ,  $Q_{12}$ ,  $P_2$ ,  $P_{21}$ , and  $Q_2$  branches, Table II lists the differences between experimental and calculated bandhead positions. The calculated bandhead positions for the (0, 0) band compare very well with experiment, considerably better than in our earlier analysis (12) which only included high  $J''$  data on two of the branches. We now have data close to the bandheads in all six branches which form bandheads, including some  $Q_{12}$ -branch members that are above the bandhead. The agreement between theory and experiment deteriorates progressively as  $v$  increases but is still good until above  $v = 18$  (see Table II). Calculations of the bandhead positions of each branch show that as  $v$  increases the  $J''$  value at the bandhead decreases.

The derived set of Dunham coefficients can be used to predict the wavenumbers of rovibronic transitions of the other isotopomers of BaI. Only  $^{127}\text{I}$  exists naturally, with mass 126.9044 and spin 5/2. Five barium isotopes have natural abundances greater than 1%, as given in Table IV. Transitions that can be attributed to isotopomers other than  $^{138}\text{BaI}$  have been observed. A regular sequence of lines has been recorded in the (0, 0)  $P_{12}$  and  $P_2$  branches that coincide with the predicted line positions of  $^{136}\text{BaI}$ . In the vicinity of  $18535.0\text{ cm}^{-1}$  the  $P_2$  (372.5) line of  $^{136}\text{BaI}$  is between the  $P_2$  (374.5) and  $P_2$  (375.5) lines of  $^{138}\text{BaI}$ .

More pronounced is the isotopic shift of bandheads. The effect on (0, 0)  $P_{12}$  and  $P_2$  is easiest to observe because the shifted bandheads appear before the onset of branches of the most abundant isotopomer. Figure 4b shows the (0, 0)  $P_2$  bandheads for  $^{138}\text{BaI}$ ,  $^{136}\text{BaI}$ , and  $^{134}\text{BaI}$ . All six bandheads for  $^{136}\text{BaI}$  and five for  $^{134}\text{BaI}$  have been observed in the (0, 0) band, and the isotopic shifts are given in Table V. Isotopic shifts were calculated using  $\rho$  values given in Table IV, where  $\rho$  is defined as  $(\mu/\mu^i)^{1/2}$ ,  $\mu$  is the reduced mass of  $^{138}\text{BaI}$ , and  $\mu^i$  is that of the isotopomer of interest. The following powers of  $\rho$  were used to adjust the Dunham coefficients: 0 for  $\Delta v$ ,  $A_{00}$ ; 1 for  $A_{10}$ ,  $Y_{10}$ ; 2 for  $A_{20}$ ,  $A_{01}$ ,  $Y_{20}$ ,  $Y_{01}$ ,  $p_{00}$ ,  $\gamma_{00}$ ; 3 for  $A_{11}$ ,  $Y_{11}$ ,  $p_{10}$ ,  $\gamma_{01}$ ; 4 for  $A_{21}$ ,  $A_{02}$ ,  $Y_{21}$ ,  $Y_{02}$ ,  $q_{00}$ ,  $p_{01}$ ,  $\gamma_{01}$ ; 5 for  $Y_{12}$ ,  $q_{10}$ ,  $p_{11}$ ; 6 for  $Y_{22}$ ,  $Y_{03}$ ,  $q_{01}$  (22). The calculated shifts are also presented in Table V. The agreement is good though there appears to be a small constant offset. The relative intensities of those bandheads follow the order of natural abundance of the corresponding Ba isotopes, but the bandheads of the less

TABLE IV  
Properties of Naturally Occurring Ba Isotopes and BaI Isotopomers

Isotope	Abundance %	Atomic Mass (amu)	$\mu(\text{BaI})$ (amu)	$\rho$	$\Gamma$
$^{130}\text{Ba}$	0.1	129.9062	64.1939	1.014647	0
$^{132}\text{Ba}$	0.1	131.9057	64.6784	1.010839	0
$^{134}\text{Ba}$	2.4	133.9043	65.1552	1.007134	0
$^{135}\text{Ba}$	6.6	134.9056	65.3914	1.005313	3/2
$^{136}\text{Ba}$	7.9	135.9044	65.6251	1.003521	0
$^{137}\text{Ba}$	11.2	136.9055	65.8577	1.001748	3/2
$^{138}\text{Ba}$	71.7	137.9055	66.0881	1.000000	0

TABLE V

Experimental Bandhead Shifts of  $^{136}\text{BaI}$  and  $^{134}\text{BaI}$  Relative to  $^{138}\text{BaI}$  and Differences from Calculated Shifts

Branch	(138)-(136)		(138)-(134)	
	Expt ( $\text{cm}^{-1}$ )	Expt-Calc. ( $\text{cm}^{-1}$ )	Expt ( $\text{cm}^{-1}$ )	Expt-Calc. ( $\text{cm}^{-1}$ )
$P_{12}$	0.1125	-0.0034	0.2314	-0.0035
$P_1$	0.0337	-0.0031	0.0718	-0.0029
$Q_{12}$	0.0265	-0.0062	0.0640	-0.0022
$P_2$	0.1147	-0.0033	0.2374	-0.0018
$P_{21}$	0.0264	-0.0024	0.0554	-0.0030
$Q_2$	0.0210	-0.0037		

abundant isotopomers appear stronger than expected.  $P_2$  and  $P_{21}$  bandheads of higher ( $v, v$ ) bands have been observed, but no detailed study has been attempted.

None of the observed transition wavenumbers could be assigned to  $^{137}\text{BaI}$  or  $^{135}\text{BaI}$ . We believe this absence is because odd-mass Ba isotopes have nuclear spin 3/2 so that hyperfine coupling would split each energy level into four. Although no Ba hyperfine coupling constants are available for any  $\text{BaX}$  ( $X = \text{F, Cl, Br}$ )  $C^2\Pi$  state, the largest hyperfine interaction of the  $\text{BaX } X^2\Sigma^+$  state arises from the Fermi contact constant, that has an average value of 2307 MHz (23). In the event that the energy level splitting in the  $C^2\Pi$  state were negligible compared to that of the  $X^2\Sigma^+$  state, adjacent hyperfine components of  $C^2\Pi-X^2\Sigma^+$  rovibronic transitions would be separated by approximately  $0.04 \text{ cm}^{-1}$ . The unobserved transitions could coincide with those of other isotopomers. Such coincidences could account for the high intensities of the bandheads for low abundance isotopomers.

To summarize, we have measured the  $\Delta v = 0$  progression in the  $\text{BaI } C^2\Pi-X^2\Sigma^+$  band system for  $v \leq 12$  with rotational resolution. The data have been analyzed in a single weighted nonlinear least-squares fit to obtain Dunham-type spectroscopic constants. These constants should allow the assignment of any set of consecutive branch members in the  $P_{12}$ ,  $R_1$ ,  $P_2$ , and  $R_{21}$  branches of the  $\Delta v = 0$  band up to at least  $v = 16$  and probably to even higher  $v$ .

#### ACKNOWLEDGMENTS

C.A.L. thanks the SERC for a NATO postdoctoral fellowship. This work is supported under NSF CHE 90-07939.

RECEIVED: September 27, 1991

#### REFERENCES

1. K. P. HUBER AND G. HERZBERG, "Molecular Spectra and Molecular Structure, IV. Constants of Diatomic Molecules," Van Nostrand-Reinhold, New York, 1979.
2. O. H. WALTERS AND S. BARRATT, *Proc. Roy. Soc. London A* **118**, 120-137 (1928).
3. M. M. PATEL AND N. R. SHAH, *Ind. J. Pure Appl. Phys.* **8**, 681-682 (1970).
4. M. L. P. RAO, D. V. K. RAO, P. T. RAO, AND P. S. MURTY, *Fizika* **9**, 25-29 (1977).
5. M. A. JOHNSON, C. NODA, J. S. MCKILLOP, AND R. N. ZARE, *Can. J. Phys.* **62**, 1467-1477 (1984).
6. C. NODA, J. S. MCKILLOP, M. A. JOHNSON, J. R. WALDECK, AND R. N. ZARE, *J. Chem. Phys.* **85**, 856-864 (1986).
7. C. A. LEACH, A. A. TSEKOURAS, P. H. VACCARO, R. N. ZARE, AND D. ZHAO, *Faraday Discuss. Chem. Soc.* **91**, 183-190; P. H. VACCARO, A. A. TSEKOURAS, D. ZHAO, C. A. LEACH, AND R. N. ZARE, *J. Chem. Phys.*, in press.

8. M. A. JOHNSON, C. W. WEBSTER, AND R. N. ZARE, *J. Chem. Phys.* **75**, 5575-5577 (1981).
9. M. A. JOHNSON AND R. N. ZARE, *J. Chem. Phys.* **82**, 4449-4459 (1985).
10. C. A. LEACH, J. R. WALDECK, C. NODA, J. S. MCKILLOP, AND R. N. ZARE, *J. Mol. Spectrosc.* **146**, 465-492 (1991).
11. C. LINTON, *J. Mol. Spectrosc.* **69**, 351-364 (1978); M. DULICK, P. F. BERNATH, AND R. W. FIELD, *Can. J. Phys.* **58**, 703-712 (1980).
12. D. ZHAO, P. H. VACCARO, A. A. TSEKOURAS, C. A. LEACH, AND R. N. ZARE, *J. Mol. Spectrosc.* **148**, 226-242 (1991).
13. T. TÖRRING AND K. DÖBL, *Chem. Phys. Lett.* **115**, 328-332 (1985).
14. P. H. VACCARO, D. ZHAO, A. A. TSEKOURAS, C. A. LEACH, W. E. ERNST, AND R. N. ZARE, *J. Chem. Phys.* **93**, 8544-8556 (1990).
15. S. GERSTENKORN AND P. LUC, "Atlas du Spectre d'Absorption de la Molécule d'Iode," Centre National de la Recherche Scientifique, Paris, 1978; S. GERSTENKORN AND P. LUC, *Rev. Phys. Appl.* **14**, 791-794 (1979).
16. R. N. ZARE, A. L. SCHMELTEKOPF, W. J. HARROP, AND D. L. ALBRITTON, *J. Mol. Spectrosc.* **46**, 37-66 (1973).
17. A. J. KOTLAR, R. W. FIELD, J. I. STEINFELD, AND J. A. COXON, *J. Mol. Spectrosc.* **80**, 86-108 (1980).
18. W. E. ERNST, J. KÄNDLER, C. NODA, J. S. MCKILLOP, AND R. N. ZARE, *J. Chem. Phys.* **85**, 3735-3743 (1986); C. A. LEACH, W. E. ERNST, J. KÄNDLER, C. NODA, J. S. MCKILLOP, AND R. N. ZARE, *J. Chem. Phys.*, **95**, 9433.
19. J. H. VAN VLECK, *Phys. Rev.* **33**, 467-506 (1929).
20. J. L. DUNHAM, *Phys. Rev.* **41**, 721-731 (1932).
21. D. L. ALBRITTON, A. L. SCHMELTEKOPF, AND R. N. ZARE, in "Molecular Spectroscopy: Modern Research" (K. Narahari Rao, Ed.), Vol. II, pp. 1-67, Academic Press, New York, 1976.
22. C. H. TOWNES AND A. L. SCHAWLOW, "Microwave Spectroscopy," Dover, New York, 1975.
23. CH. RYZLEWICZ, H.-U. SCHÜTZE-PAHLMANN, J. HOEFT, AND T. TÖRRING, *Chem. Phys.* **71**, 389-399 (1982); W. E. ERNST, G. WEILER, AND T. TÖRRING, *Chem. Phys. Lett.* **121**, 494-498.